Development of a Biophysical Model of Lower Urinary Tract Function

Elliot Lister

4th Year Project Report
Computer Science and Mathematics
School of Informatics
University of Edinburgh

2024

Abstract

Lower urinary tract dysfunction significantly impacts millions globally, reducing quality of life. Limited understanding hinders the development of more effective treatments. Computational models offer a promising approach to address this gap in knowledge. This report details the implementation, validation, and development of a model of the human female lower urinary tract. A rigorous validation process was performed, including a comparison to published human female trends and a comparison to established physiological ranges. Additionally, the outputs of the model were correlated with the pressure-volume relationship from rodent bladder data, demonstrating a strong correlation coefficient of 0.93. This successful development paves the way for future integration with neural circuit models.

Research Ethics Approval

This project was planned in accordance with the Informatics Research Ethics policy. It did not involve any aspects that required approval from the Informatics Research Ethics committee.

Declaration

I declare that this thesis was composed by myself, that the work contained herein is my own except where explicitly stated otherwise in the text, and that this work has not been submitted for any other degree or professional qualification except as specified.

(*Elliot Lister*)

Acknowledgements

I would like to thank Professor Kia Nazarpour and Aidan McConnell-Trevillion for introducing me to the world of biophysical modelling and neuromodulatory approaches for treating lower urinary tract dysfunction. I am especially grateful to Aidan for his ongoing mentorship and support throughout the project. His willingness to answer my questions, both within and outside the scope of the research, has been invaluable and will undoubtedly benefit my future academic career.

Table of Contents

Chapter 1

Introduction

1.1 Motivation

Lower urinary tract symptoms (LUTS) are highly prevalent, affecting over 60% of adults by the age of 40 [1]. Overactive bladder (OAB) is a type of storage LUTS [2] that affects millions of people worldwide and is characterised by urinary urgency, frequency, and urge incontinence [3]. According to a study conducted in 2011, approximately 10.7% of the global population was impacted by OAB, with further increases expected [4]. In the United Kingdom, it is estimated that 12% of the population have OAB [3], although the true figure could be higher as many cases go unreported due to social stigma [5]. Moreover, OAB can have a significant impact on quality of life, causing social embarrassment, sleep disruption, and anxiety [5].

Despite the availability of treatments for OAB, such as bladder retraining and medications [6], limited knowledge about the underlying mechanisms remains a barrier to developing more efficient solutions with fewer side effects. This knowledge gap can be addressed by developing computational models of the lower urinary tract (LUT).

Modelling of the LUT enables clinicians and researchers to construct simulated organs that integrate individual patient characteristics and different states of disease. This personalised approach enables the prediction of treatment outcomes under different scenarios, guiding the selection of the most effective treatment strategy. As an example, a model could emulate how medication, surgery, or lifestyle changes influence urinary function. Clinicians can use the results to make informed choices about the most effective treatment for a particular patient. By minimising time spent trialling ineffective treatment plans, valuable time and resources can be conserved. Given the £840 million that the UK is currently spending on OAB patients each year through the NHS [7], this becomes particularly advantageous.

Moreover, models play a significant role in designing and optimising medical devices. One instance is tibial neuromodulation, which provides a minimally invasive therapy for LUT dysfunction, such as OAB. It works by stimulating the posterior tibial nerve in the ankle, which modulates the sacral nerves in the spinal cord responsible for controlling bladder function [8]. Integrating a model of the LUT can simulate the effects of

tibial neuromodulation on individual patients, helping to predict treatment response and optimise stimulation parameters. This approach has already been successfully implemented within the lab. The work presented in this report could further ongoing research by providing valuable data generation to refine these models and improve their accuracy for clinical application.

Finally, the LUT is a highly intricate system, and its dysfunction can stem from various factors. By utilising biophysical models, researchers can systematically study the pathophysiology of the LUT. This involves the exploration of the underlying mechanisms of urinary tract disorders, including the interplay between various physiological parameters, such as bladder pressure, urethral resistance, and neural control.

1.2 Aims and objectives

Aim 1: Conduct a literature review of current techniques used in the biophysical modelling of the LUT.

- **Objective 1.1:** Identify existing biophysical models used for simulating the LUT.
- **Objective 1.2:** Analyse the strengths and limitations of current approaches.

Aim 2: Implement and validate a biophysical model of the LUT

- **Objective 2.1:** Implement a selected biophysical model of the LUT identified in the literature review.
- **Objective 2.2:** Evaluate the model's functionality by simulating various physiological scenarios.
- **Objective 2.3:** Validate the model's accuracy by comparing its simulated outputs with reported physiological results.

1.3 Contributions

Within this project, the following contributions are presented:

- A novel and complete implementation of the Bastiaanssen et al. model [9]. Despite providing a valuable foundation, Bastiaanssen's work did not offer a complete and reproducible model or any accompanying code. This report bridges that gap by creating a functional open-source model which can be used by the lab to explore LUT neuromodulatory therapies in a simulated environment.
- A rigorous model validation through comparisons to established benchmarks: published human trends, known physiological ranges, and pressure-volume relationships from rodent bladder experiments.
- An extension beyond the existing model. By incorporating physiological features like circadian rhythm in the kidney function and noise injection, the model captures the natural fluctuations in urine production and inherent variability within the LUT, resulting in a more realistic model which outperforms the original.

Chapter 2

Background

2.1 Biology of the Lower Urinary Tract

While this project focuses on implementing a computational model, a foundational understanding of the biological system is necessary for several reasons. Firstly, the LUT refers to a complex group of interconnected organs and nerves involved in urine storage and voiding (release). The complexity of the LUT requires a focus on essential components in order to achieve a model that can be validated and run efficiently. Learning about its biology helps to identify these components and replicate LUT function at a level relevant to the model's purpose.

Gaining knowledge of the biological mechanisms also enables the establishment of feasible parameter ranges. In the absence of these limits, the model's behaviour could become unrealistic and deviate from the actual physiological processes.

Understanding the physiology and innervation is important when defining interactions between components. By comprehending the way certain LUT interact with each other, such as the nerves and muscles in the bladder, the model can accomplish a more accurate and physiologically meaningful representation of the LUT's function.

The LUT consists of three main components: the bladder, the urethra, and the neural control system [10]. Sex differences exist in LUT physiology and this project specifically focuses on a female bladder model, due to the greater prevalence of female models in existing literature. Certain parameters, such as urethral length, may differ between sexes [11], however, the core functional components remain similar and will be the focus of this discussion.

2.1.1 Bladder

The bladder is a muscular organ innervated by somatosensory and motor neurons responsible for storing urine [12]. Ascending sensory (afferent) nerves originating from the bladder send signals to the brain about the volume of urine while descending (efferent) motor nerves send signals from the brain to the bladder to control contractions [13]. The main bladder muscle involved in micturition is the detrusor, a smooth muscle

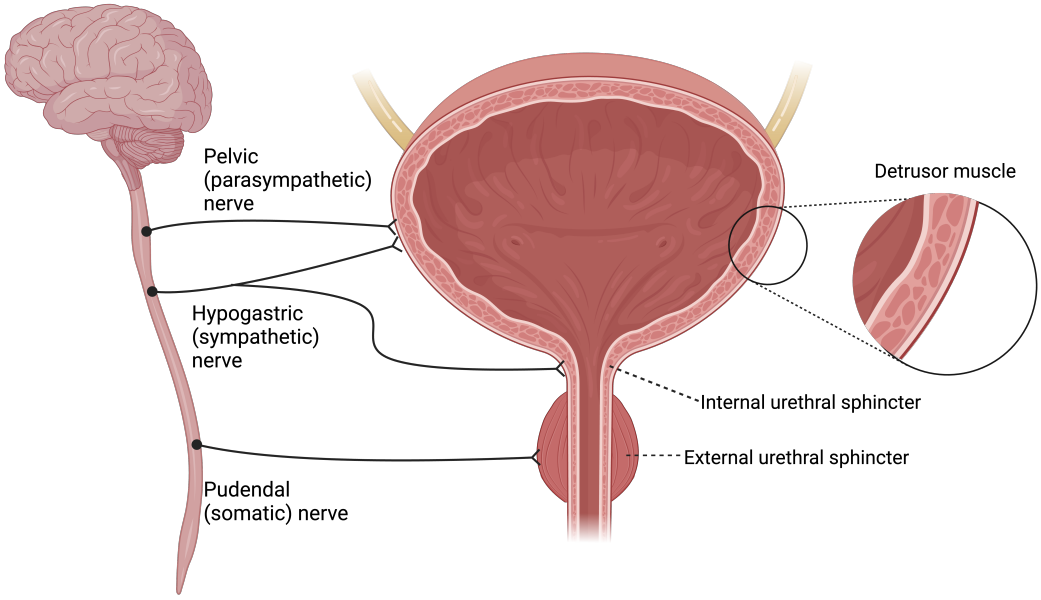

Figure 2.1: Anatomy of the lower urinary tract, highlighting the detrusor, urethral sphincters, and their innervation, created with BioRender.com [16]

comprised of interlacing fibres which contracts involuntarily to force urine out of the bladder into the urethra, or relaxes to allow for storage [14]. In addition to the smooth muscle that contracts involuntarily, the LUT also relies on striated muscle within the urethra for voluntary control [15].

2.1.2 Urethra

The urethra is a collapsible tube that extends from the bladder neck and comprises both smooth and striated muscle, and contains two sphincters which facilitate or prevent the transport of urine out of the body [10]. The internal urethral sphincter is a smooth muscle that is responsible for maintaining continence during the storage phase of the bladder by involuntarily contracting and promoting urination by relaxation during the voiding phase [15]. Comprised of striated muscle, the external urethral sphincter is situated at the distal inferior end of the bladder [15]. Due to its composition of striated muscle, the external sphincter enables voluntary control through contraction or relaxation, unlike the smooth muscle of the internal sphincter [15].

2.1.3 Neural control

The three nerves of importance to micturition (urination) are the pelvic nerve, the hypogastric nerve, and the pudendal nerve [12]. These nerves work together to coordinate storage and voiding of urine from the bladder.

Stimulation of the pelvic nerve results in the contraction of the detrusor muscle [12]. During micturition, the pelvic nerve sends signals to the detrusor muscle, causing it to

contract and expel urine from the bladder.

When the hypogastric nerve is stimulated, it leads to the contraction of the bladder neck and urethra. Additionally, it helps relax the detrusor muscle and counteracts the pelvic nerve during storage [12]. During storage, the hypogastric nerve helps prevent urine from leaking out of the bladder by keeping the bladder neck and the internal urethral sphincter closed.

The external urethral sphincter is under the control of the pudendal nerve [12]. While in the storage phase, stimulation of the pudendal nerve causes the contraction of the external urethral sphincter, preventing the flow of urine from the urethra.

The anatomical details of the lower urinary tract (LUT), with emphasis on its aforementioned key components and their innervation, are summarised in Figure 2.1.

2.2 Description of the neural circuit

The existing Python code, developed by another member of the lab, simulates a neural circuit model of the lower urinary tract. The model is based on the topology described in the previous work by de Groat and Wickens [17], in which the LUT has three efferent and afferent neurons, each to and from the bladder, internal sphincter, and external sphincter.

The neural activity underlying micturition has been studied in animals, and so the current bladder model uses pre-recorded neural data from rats displaying normal bladder function [18]. This data comprises a set of pressure and volume measurements taken at independent time intervals. These measurements are interpolated to generate data points for each time step in the simulation run. However, this approach does not allow for causal data beyond the finite recorded set. In other words, it is not possible to use the model to investigate the effects on bladder function when altering neural inputs, or to extend the temporal range of the data. The aim of this project is to implement a LUT model that is generates outputs similar to the recorded values (bladder pressure and volume). This project lays the groundwork for future integration of the model, enabling continuous data generation for unrestricted studies and a deeper understanding of the circuit's function under neural perturbations.

2.3 Model selection

The choice of model is important for the success of any study investigating the mechanisms of LUT function and dysfunction. In this section, the different leading models will be discussed and evaluated in relevance for this project.

Currently, there is no comprehensive LUT model that caters to all purposes. Instead, the present research emphasises the utilisation of modular components that specialise in particular parts of the LUT [10].

In order to make a model selection, a set of criteria was defined. Firstly, the model must be able to receive input from the neural circuitry that controls bladder function. This

will allow the model to simulate the effects of changes in neural activity on bladder function. In addition to receiving neural input, the model must also be able to calculate bladder pressure and volume, either directly or by using an intermediate calculation. This will allow the model to simulate changes in bladder pressure and volume that occur during storage and voiding. The best model from the remaining will be the one that is computationally efficient and generates realistic results comparable to the recorded data.

After reviewing several models of the lower urinary tract, the model by Bastiaanssen et al. [19] was selected. The primary advantage of this model lies in its support of the three neural inputs, facilitating seamless integration into the ongoing work within the lab at a later phase. Additionally, this model accurately represents the structure of the striated muscle found in the external urethral sphincter. Besides incorporating more physiological accurate elements, this addition also simplifies clinical investigations into urethral obstruction or bladder hypertonicity [9].

One of the alternative models considered was the Valentini, Besson, and Nelson (VBN) model [20]. With its detailed mathematical representations of the micturition process, the VBN model has emerged as one of the predominant models in the field. However, it is not as best suited as it does not describe reproducible mathematics behind the system, nor does it publicly share open-source code. The lack of accessible code is a prevailing issue in LUT modelling, as highlighted in a recent review, which found that none of the prominent models use online repositories to share code [10].

The models by Hosein and Griffiths [21] and van Duin [22] are simpler than the Bastiaanssen model. However, their portrayal of urethral mechanics is described as an adjustable resistance, which overlooks the physiological details presented in the Bastiaanssen model, thus reducing their accuracy.

Furthermore, the model implemented by Fletcher [23] (previously designed by Hübener et al. [24]), is thoroughly documented from a mathematical standpoint, akin to Bastiaanssen's work. However, it suffers from the same lack of detail in the urethra as the other models. In addition to the missing urethral dynamics, the nerve signals are modelled by only two equations:

$$s_1 = 1 - e^{-k_1 t} \qquad s_2 = (1 - C)e^{-k_2 t} + C \tag{2.1}$$

This would require further work to map the three inputs/outputs of the existing circuitry described in section 2.2 into two nerve signals provided in the model. Consequently, Bastiaanssen's model outperforms the models proposed by Hosein and Griffiths, van Duin, and Hübener in terms of suitability for modelling in this particular case.

Finally, Paya et al. [25] have presented a model that shows similarities with the work of Bastiaanssen. In contrast, this model includes a more comprehensive representation of the afferent signals originating from the internal urethral sphincter [25]. However, this increased detail comes at the cost of greater complexity in the neuronal representation, which is unnecessary for the research that the model will be used for. The additional complexity would also make validation more challenging with the current resources. Hence, the decision was made to not proceed with this method.

Chapter 3

Methods

This section provides an overview of the framework and verification methods used in the LUT model. The description begins with the model's core principles and high-level methodologies. Following that, a computational outline of the model's implementation is given, along with a flowchart. Finally, the methodologies used to assess the validity and performance of the model are described. Detailed mathematical descriptions and pseudocode implementation will be presented in chapter 4.

3.1 Model description

The Bastiaanssen model [19] starts by inputting three normalised neural inputs: ω_e^* for the excitatory input of the detrusor, ω_i^* for the inhibitory input of the detrusor, and ω_s^* for the excitatory input of the sphincter. These relate to the pelvic, hypogastric, and pudendal nerves, respectively, as shown in Figure 2.1.

The remaining part of the model is centred on three state variables:

- V_B: The volume within the bladder.
- f_{aD}^*: The normalised activation of the detrusor
- f_{aS}^*: The normalised activation of the sphincter

Each state variable is modelled and updated by a differential equation, where the neural activations make use of time constants τ_D and τ_S. The paper refers to the functions that model each equation as f_1, f_2, and f_3, respectively:

$$\begin{aligned} \frac{\mathrm{d}V_B}{\mathrm{d}t} &= f_1(f_{aD}^*, V_B, Q) = Q_{\text{in}} - Q \\ \tau_D \frac{\mathrm{d}f_{aD}^*}{\mathrm{d}t} &= f_2(f_{aD}^*, \omega_e^*, \omega_i^*) = \omega_e^* - f_{aD}^* - \omega_i^* f_{aD}^* \\ \tau_S \frac{\mathrm{d}f_{aS}^*}{\mathrm{d}t} &= f_3(f_{aS}^*, \omega_s^*) = \omega_s^* - f_{aS}^* \end{aligned} \tag{3.1}$$

However, whilst the normalised activations of the detrusor and sphincter are updated using their prior values and the neural inputs, the volume is determined by Q_{in} and

Q, the bladder inflow and outflow of urine. Urine inflow, Q_{in}, is always either a fixed constant or zero (if there is high fluid pressure in the bladder, blocking inflow from the kidneys). Consequently, the primary aim of this model is to compute the outflow of urine, Q, at each time step.

Q is modelled as an expression of the urethral opening radius, r_U, and the state variables. The urethral radius, r_U can be determined by analysing the flow characteristics within the urethra. An implicit relationship exists that defines r_U. This relationship can be expressed as a function, $f_0(V_B, f^*_{aD}, f^*_{aS}, r_U)$. The root of this function is found using the bisection method and provides the value of r_U. Within the simulation model, a mapping function, f_{map}, is used to describe r_U based on the other state variables.

3.2 Implementation

Computationally, this model was implemented in Python as shown in Figure 3.1. This implementation differs from the existing model by including a basic neural network model that updates the neural inputs. Bastiaanssen's neural model, as described in a previous paper [26], does not offer enough specifics about its fitting procedure and data sources, rendering it non-reproducible. Consequently, the approach involves utilising a piecewise function that emulates the observed behaviours outlined in the paper.

3.3 Validation methodology

The validation of data generated by the LUT model is an essential step in ensuring safe deployment of the model. Neuromodulation relies on manipulating the nervous system's activity, and inaccurate outputs could have unintended consequences when are being deployed in medical therapies.

The majority of LUT models do not use contextually appropriate data when validating [10]. There are various limitations that can cause this. Firstly, the acquisition of human data can present ethical challenges. Additionally, the use of low-resolution equipment can hinder the accurate representation of the biological processes targeted by the model [9]. Finally, achieving comprehensive validation would require testing against a range of individuals. Conducting the assessment of all the necessary parameters for the model can take a substantial amount of time and money when using a larger sample size.

Given the time limitations of this project, it was not possible to obtain human data. Hence, the approach to validation is to compare the model with:

- Published results of human data. While the data is not publicly accessible, the model's results will be visually compared with existing findings.
- Physiological ranges of components. Model outputs will be checked to see if they are within established physiological ranges.
- Data recorded from rats. Although it cannot replace human data, it can contribute valuable quantitative insights to evaluate the model's accuracy.

This approach seeks to ensure that the model is consistent with existing scientific knowledge and established physiological bounds, even in the absence of human data.

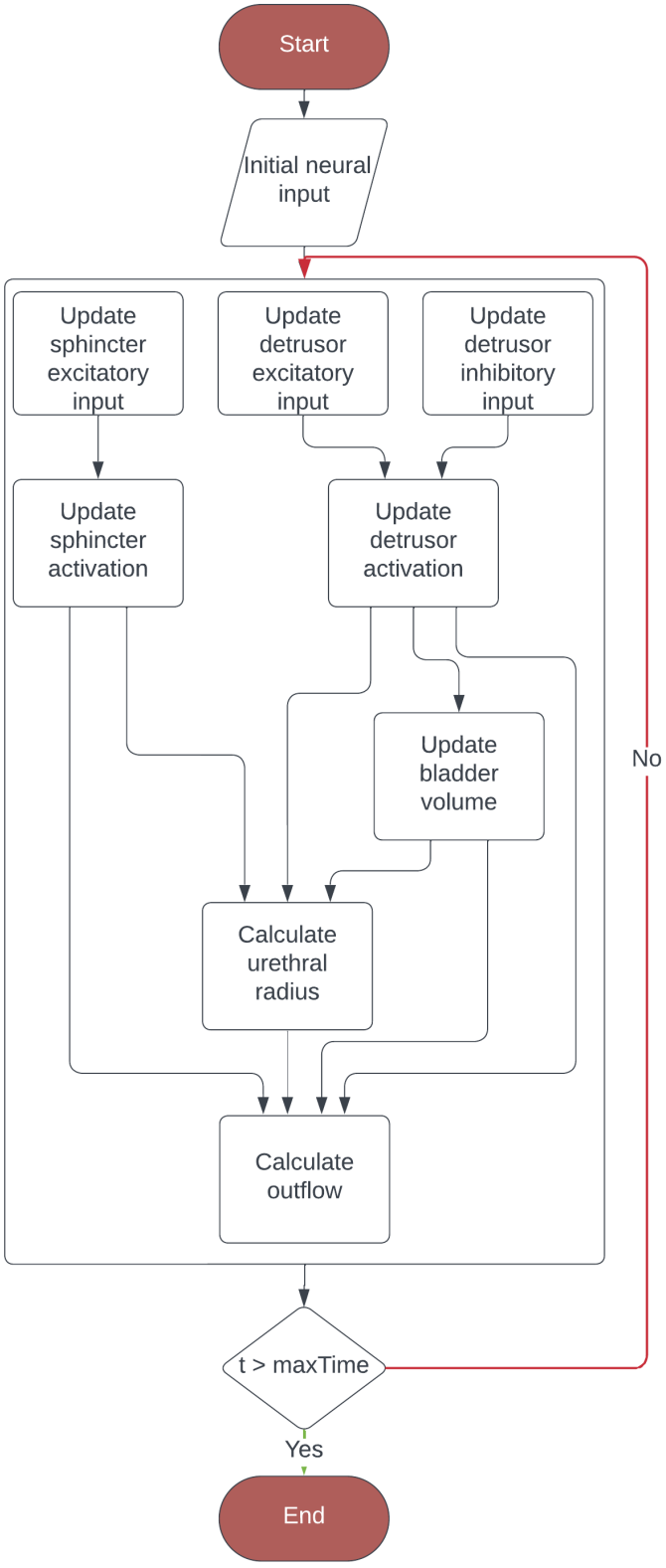

Figure 3.1: Outline of the model's structure

Chapter 4

Implementation

This chapter describes the implementation of the mathematical model outlined by Bastiaanssen, adopting a sequential format, closely resembling the model illustrated in Figure 3.1. Every section represents a fundamental component of the algorithm and will be summarised through pseudocode algorithms as needed.

4.1 Neural control model

In section 3.2, it was stated that the neural control model mentioned in the original source could not be replicated because of insufficient data and descriptions of fitting techniques. Instead, the model was simulated using piecewise functions as displayed below:

As seen in Algorithm 1 both excitatory and inhibitory detrusor neural inputs increase linearly with bladder volume, where the excitatory input has a greater weight. This difference between inputs results in an accelerated neural response per unit volume. Upon voiding, the excitatory input increases to 1 and the inhibitory input decreases to 0, resulting in a maximum contraction of the detrusor (see Figure 4.1b). Conversely, the sphincter input has a constant value which relaxes upon voiding (see Figure 4.1b).

The purpose of these functions is not to replicate the system exactly, but rather to serve as a simplified approximation for implementing and validating the LUT model. If the work were to be integrated with the lab's existing circuit model, the weights would be calibrated.

Algorithm 1 Neural control model

function UPDATE SYMPATHETIC INPUT(V_B, voiding)
    if voiding **then return** 0
    else
        $k = 0.5$ **return** $\max\left(k\frac{V_B}{V_{\max}}, 0.1\right)$
    end if
end function

function UPDATE PARASYMPATHETIC INPUT(V_B, voiding)
    if voiding **then return** 1
    else
        $k = 0.075$ **return** $k\frac{V_B}{V_{\max}}$
    end if
end function

function UPDATE SOMATIC INPUT(V_B, voiding)
    if voiding **then return** 0.05
    else
        return 0.5
    end if
end function

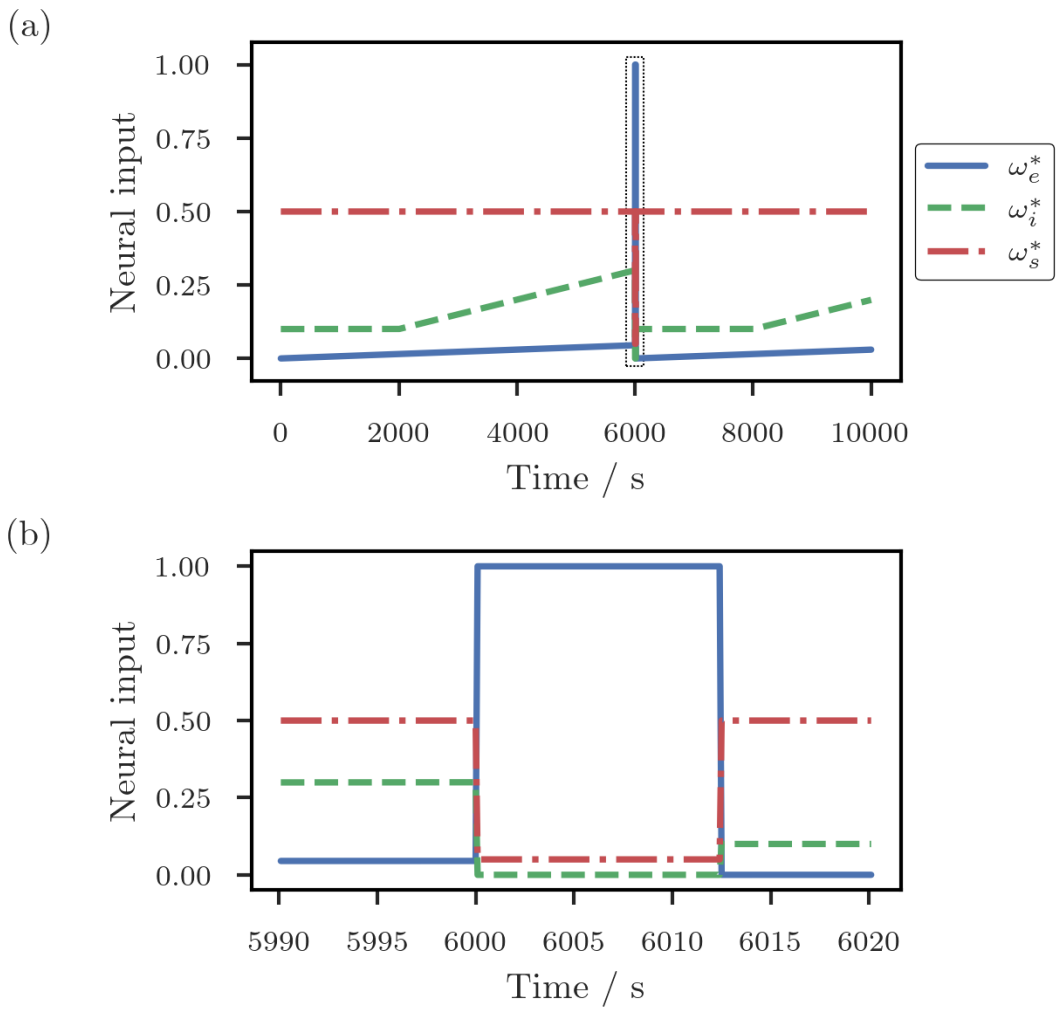

Figure 4.1: Excitatory (ω_e^*) and inhibitory (ω_i^*) detrusor neural inputs and sphincter neural input (ω_s^*) during full storage and voiding cycle (a), with the voiding event highlighted by a dotted rectangle. The same cycle is magnified on the voiding event (b).

4.2 Detrusor and sphincter activation

Rearranging the functions, f_2 and f_3 described in section 3.1, the normalised activations of the detrusor and sphincter were calculated, as shown in Figure 4.2. During voiding, the activation of the muscles in the bladder wall increases, resulting in greater contraction, while the sphincter relaxes.

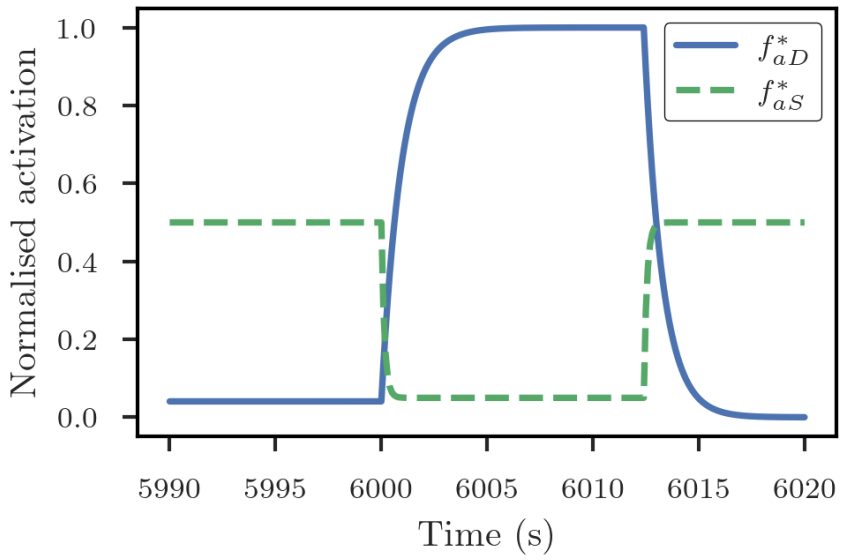

Figure 4.2: Normalised activation of the detrusor f^*_{aD} and sphincter f^*_{aS} during voiding.

4.3 Calculating urethral radius

4.3.1 Equilibrium of forces in the urethra, f_{map}

Initially, it is assumed that there is a known flow of urine out of the bladder (defaults to $Q = 0$). However, the rate at which urine flows out subsequently depends on the opening of the urethra. Increasing the radius of this opening will cause a higher outflow, whereas closing the opening will cause the outflow to decrease until it stops completely.

The f_{map} function accepts three arguments, namely V_B (bladder volume), f^*_{aD} (normalised detrusor activation), and f^*_{aS} (normalised sphincter activation). This function identifies a value for r_U (urethral radius) that meets a specific condition regarding pressure differences. Internally, f_{map} utilises a numerical bisection optimisation technique. In the Python implementation of the model, the bisection method was achieved using the SciPy package [27]. This method iteratively refines its guess for r_U by evaluating a function (f_0) with different r_U values within a range (0 m to 0.005 m). f_0 calculates the pressure difference ($p_T - p_S$) between the entrance of the urethra (p_T) and the sphincter (p_S). The bisection method is used to calculate the root of the function f_0, which signifies the point at which pressures are equal, thereby indicating the radius of the urethra. In cases where the bisection method fails to locate a root, it defaults to assigning a value of zero to r_U, under the assumption that the urethra remains closed

(see Algorithm 2).

Algorithm 2 f_{map}

function $f_{\text{map}}(V_B, f^*_{aD}, f^*_{aS})$
  $r_U \leftarrow \text{bisect}\left(r_U : f_0(V_B, f^*_{aD}, f^*_{aS}, r_U), 0, 5 \times 10^{-3}\right)$
  if no solution found **then**
    $r_U \leftarrow 0$
  end if
return r_U
end function

4.3.2 Active tensile stress-length relationship for striated muscles

Before establishing the objective function f_0, it is necessary to define key relationships, starting with the force-length relationship for striated muscles.

Contraction in striated muscles, such as those found in the sphincter and detrusor, is achieved through the use of sarcomeres, which serve as the fundamental contractile units of striated muscle fibres [28]. Specialised protein filaments, namely actin and myosin, are arranged in a repeating pattern within the sarcomeres. These filaments interact with each other to produce the force that leads to muscle contraction.

The sliding filament theory explains the generation of force by sarcomeres. According to this theory, the actin and myosin filaments show sliding movement when contracting [28]. The force generated by the sarcomere is determined by the extent of overlap between the filaments. Maximum force generation in the sarcomere occurs when the overlap is at its optimal level. However, excessive stretching or compression of the sarcomere results in a reduced filament overlap, which causes a decrease in the production of force [29].

The force-length relationship can be applied to both the detrusor and sphincter. In these striated muscle tissues, the normalised isometric active tensile stress is related to the normalised radius of curvature of the bladder/sphincter. The radius of curvature reflects stretch or compression in the muscle. When the normalised radius of curvature is optimal, the muscle can generate maximum force. In the model, this is used implicitly within the relationship between curvature radius and sarcomere length:

$$l_D = \frac{l_{\text{opt}D}}{r_{\text{opt}D}} r_D \quad l_S = \frac{l_{\text{opt}S}}{r_{\text{opt}S}} r_S \tag{4.1}$$

Although the original paper established a solid basis for the LUT model, certain essential relationships were not explicitly described mathematically. To tackle this problem, non-linear functions were reconstructed by analysing the presented data [9] and validating physiological principles against other experimental results [29]. Subsequently, the mathematical functions were reconstructed and transcribed into the Python code. This approach successfully captures the fundamental concept of the LUT system, even without explicit reference to the specific formulas outlined in the original paper.

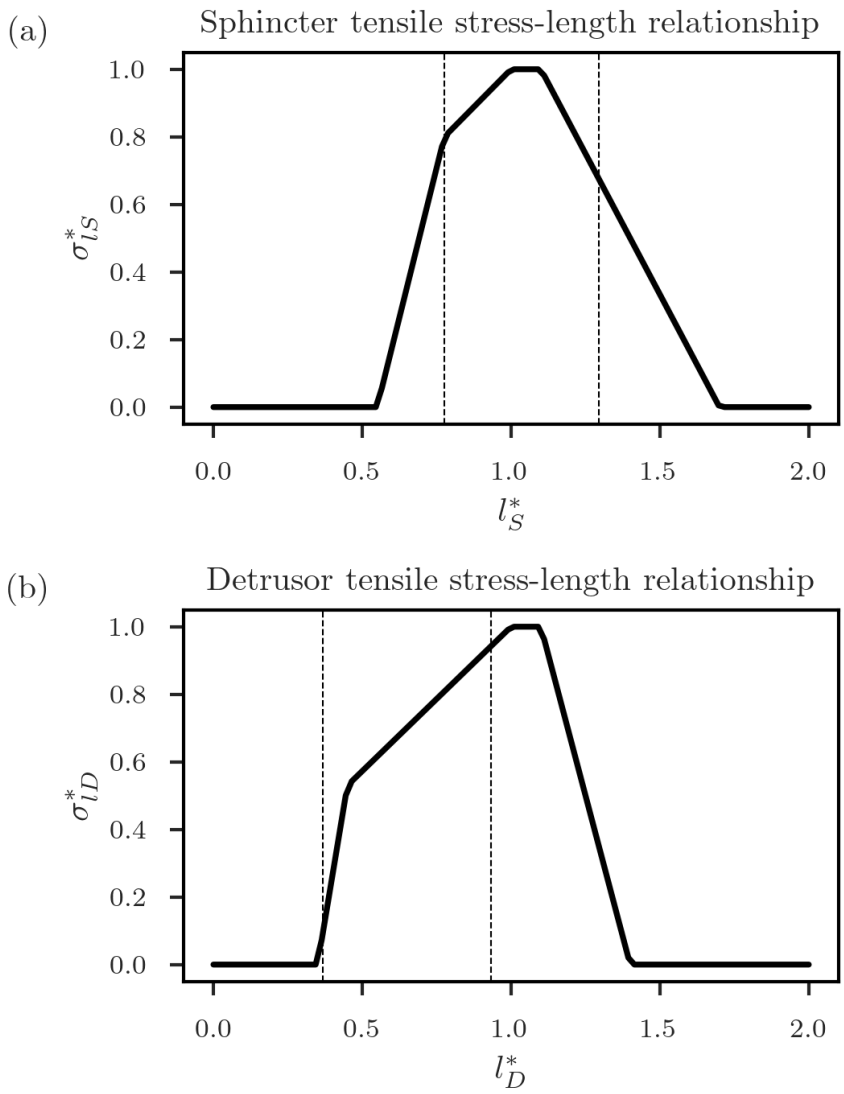

Figure 4.3: Active tensile stress-length relationship for the sphincter and detrusor. Operational bounds are denoted by vertical dashed lines. σ^*_{lS} and σ^*_{lD} represent the normalised tensile stress in the sphincter and detrusor.

4.3.3 Active force–velocity relationship for striated muscles

Another key relationship is the effect of contraction velocity on tensile stress. The Hill equation [30] can be used to describe the force-velocity relationship of striated muscles during shortening. This equation relates the normalised active force (σ^*_u) developed by the muscle to its normalised shortening velocity (u^*). The Hill curve can be defined by two muscle-specific parameters, namely k (a constant) and $u_{\max}$ (the maximum attainable normalised velocity).

The Hill equation is only valid for shortening ($u^* > 0$) [29], whereas a separate relationship, established through experimental data [31], is used for lengthening ($u^* < 0$) of muscle fibres in the LUT model as presented in Bastiaanssen [9].

Here, the relationship between u* and the normalised stress (σ_s^*) at the optimal muscle fibre length is expressed as follows:

$$\sigma_s^*(u^*) = \begin{cases} 1.8 - \frac{0.8(1+u^*)}{1-7.56u^*/k} & \text{if } u^* < 0 \text{ (lengthening)} \\ 1 & \text{if } u^* = 0 \text{ (isometric contraction)} \\ \frac{1-u*}{1+u^*/k} & \text{if } u^* > 0 \text{ (shortening)} \end{cases} \tag{4.2}$$

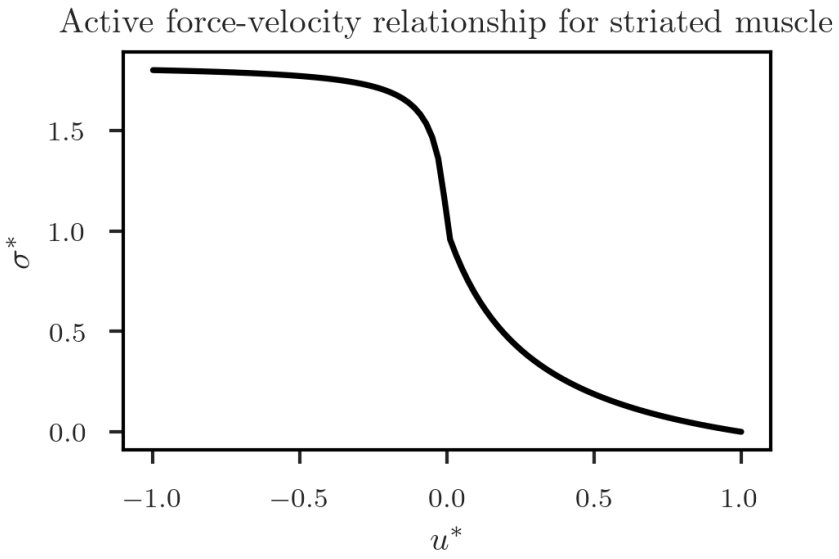

Figure 4.4: Active tensile stress-velocity relationship for the striated muscles

4.3.4 Sphincter pressure

Active tension is muscle tension that results from a neural stimulus, whereas passive tension is caused by elastic potential stored during muscle stretching, regardless of the presence of a stimulus. The total pressure at the inner side of the sphincter is influenced by both the active and passive components.

The passive component is modelled by an exponential relationship dependent on the urethral radius r_U and various physiological constants [9]:

$$p_{\text{pas}S} = p_{0S} \cdot \left(\frac{p_{\text{nom}S}}{p_{0S}} \right)^{\frac{r_U}{r_{0S}}} \tag{4.3}$$

where p_{0S} is the pressure at $r_U = 0$ (urethra fully closed) and $p_{\text{nom}S}$ is the nominal pressure when the urethra has a radius of r_{0S}, allowing the exponential model to be fit around established data points.

Active pressure within the urethra depends on the muscle tension in the sphincter wall (σ_S) and the curvature of the sphincter. Given the assumption that the sphincter can be

modeled as a cylinder, it exhibits unidirectional bending. Hence, the active pressure can be represented by the equation [9]:

$$\begin{aligned} p_{\text{act}S} &= \int_{r_{\text{in}S}}^{r_{\text{out}S}} \frac{\sigma_{\text{act}S}}{r} \mathrm{d}r \\ &= \sigma_{\text{act}S} \ln\left(\frac{r_{\text{out}S}}{r_{\text{in}S}}\right) \end{aligned} \tag{4.4}$$

In order to calculate the active tensile stress, the model calculates the nominal active tensile stress $\sigma_{\text{nom\_act}S}$ at a known sphincter width $h_{\text{nom}S}$. The magnitude of the force exerted in the sphincter depends upon the contractual unit's length, the velocity of normalised contraction, and the activation of said unit. The model assumes a uniform activation of contractile units, allowing the utilisation of the equation for a muscle fibre [9]:

$$\sigma_{\text{nom\_act}S} = f_{aS}^{*} \cdot \sigma_{\text{isoS}} \cdot \sigma_{uS}(u_S^{*}) \cdot \sigma_{lS}^{*}(l_S) \tag{4.5}$$

The final non-geometric calculation required is to calculate the contraction velocity u_S. As the bladder fills with urine, it stretches the sphincter muscle fibers. The contraction velocity, how fast the muscle shortens, depends on the current length of the fibers (relative to their optimal length, $l_S/l_{\text{opt}S}$). The velocity at which the sphincter is closing can be determined by analysing this ratio and the rate of change [9]:

$$\begin{aligned} u_S &= \frac{-\mathrm{d}l_S/l_{\text{opt}S}}{\mathrm{d}t} \\ &= -\frac{1}{r_{\text{opt}S}} \frac{\mathrm{d}r_S}{\mathrm{d}t} \end{aligned} \tag{4.6}$$

The rate of change of r_S can be found as follows:

$$\begin{aligned} \frac{\mathrm{d}r_S}{\mathrm{d}t} &= \frac{\mathrm{d}r_S}{\mathrm{d}A_U} \frac{\mathrm{d}A_U}{\mathrm{d}r_U} \frac{\mathrm{d}r_U}{\mathrm{d}t} \\ &= \frac{\mathrm{d}(r_{\text{out}S} + r_{\text{in}S}/2)}{\mathrm{d}A_U} (2\pi r_U) \frac{\mathrm{d}r_U}{\mathrm{d}t} \\ &= \frac{r_U}{2} \left(\frac{1}{r_{\text{out}S}} + \frac{1}{r_{\text{in}S}}\right) \frac{\mathrm{d}r_U}{\mathrm{d}t} \end{aligned} \tag{4.7}$$

Hence, the contraction velocity of the sphincter is given as:

$$u_S = -\frac{r_U}{2r_{\text{opt}S}} \left(\frac{1}{r_{\text{out}S}} + \frac{1}{r_{\text{in}S}}\right) \frac{\mathrm{d}r_U}{\mathrm{d}t} \tag{4.8}$$

The derivative is approximated as the difference between urethral radii between time steps. The purpose of this approximation is to compute contraction velocity without relying on Q. The importance of this lies in its use to determine the urethral radius, which is essential for the later calculation of the flow rate, Q. To this end, introducing Q in the calculation would create a cyclical dependency.

Algorithm 3 summarises the previous derivations into a single function to calculate sphincter pressure, where any undefined variables are constants sourced from Bastiaanssen et al. [9].

Algorithm 3 p_S

function $p_S(A_U, f^*_{aS}, r_U)$

$r_{\text{out}S} = \left(\frac{1}{\pi}(A_U + A_{\text{tissue}S} + A_{\text{muscle}S})\right)^{1/2}$

$r_{\text{in}S} = \left(\frac{1}{\pi}(A_U + A_{\text{tissue}S})\right)^{1/2}$

$r_S = \frac{r_{\text{out}S} + r_{\text{in}S}}{2}$

$h_S = r_{\text{out}S} - r_{\text{in}S}$

$\frac{\mathrm{d}r_U}{\mathrm{d}t} = \frac{r_U - r_{U,(t-\Delta t)}}{\Delta t}$

$u_S = -\frac{r_U}{2r_{\text{optS}}}\left(\frac{1}{r_{\text{out}S}} + \frac{1}{r_{\text{in}S}}\right) \cdot \frac{\mathrm{d}r_U}{\mathrm{d}t}$

$u^*_S = \frac{u_S}{u_{\text{maxS}}}$

$l_S = \frac{l_{\text{optS}}}{r_{\text{optS}}} \cdot r_S$

$\sigma_{\text{nom\_act}S} = f^*_{aS} \cdot \sigma_{\text{isoS}} \cdot \sigma_{uS}(u^*_S) \cdot \sigma^*_{lS}(l_S)$

$\sigma_{\text{act}S} = \frac{h_{\text{nomS}}}{h_S} \cdot \sigma_{\text{nom\_act}S}$

$p_{\text{act}S} = \sigma_{\text{act}S} \cdot \ln\left(\frac{r_{\text{out}S}}{r_{\text{in}S}}\right)$

$p_{\text{pas}S} = p_{0S} \cdot \left(\frac{p_{\text{nomS}}}{p_{0S}}\right)^{\frac{r_U}{r_{0S}}}$

$p_S = p_{\text{act}S} + p_{\text{pas}S}$

return p_S

end function

4.3.5 Outflow in terms of urethral radius

The complete derivation for calculating the square outflow (Q^2) is beyond the scope of this discussion. However, the main concept revolves around harnessing principles of fluid dynamics to establish a relationship between the changing urethral radius (r_U) and the rate of urine flow. According to Bernoulli's principle, the velocity of a fluid is inversely proportional to its pressure [32]. By applying Bernoulli's principle to the pressure difference between the bladder neck and the urethra, the model treats the flow as analogous to a small, expanding funnel. This reflects the increasing radius as urine moves from the bladder into the urethra. The aim of this is to define a function that can ascertain the square outflow at different time intervals, based on the urethral radius (r_U). This function is presented below [9].

$$Q^2 = \frac{p_S(r_U)A^2_U(r_U)}{\frac{\rho}{2}(1 - A^2_U(r_U)/A^2_T(r_U)) + (R(r_U)A^2_U(r_U))} \tag{4.9}$$

4.3.6 Detrusor pressure

There are several parallels between the calculation method for detrusor pressure and sphincter pressure. The first notable variation is observed in the evaluation of the detrusor's contraction speed [9]:

$$u_D = -\frac{1}{r_{\text{opt}D}}\frac{\mathrm{d}r_D}{\mathrm{d}t} \tag{4.10}$$

Employing a similar approach as with the sphincter, this time using the knowledge that the volume is spherical:

$$\begin{aligned} u_D &= -\frac{1}{r_{\text{opt}D}} \frac{\mathrm{d}r_D}{\mathrm{d}V_B} \frac{\mathrm{d}V_B}{\mathrm{d}t} \\ &= -\frac{1}{r_{\text{opt}D}} \frac{\mathrm{d}((\frac{1}{r_{\text{out}D}} + \frac{1}{r_{\text{in}D}})/2)}{\mathrm{d}V_B} (Q_{\text{in}} - Q) \\ &= -\frac{1}{8\pi r_{\text{opt}D}} \left(\frac{1}{r_{\text{out}D}} + \frac{1}{r_{\text{in}D}}) \right) (Q_{\text{in}} - Q) \end{aligned} \tag{4.11}$$

However, considering the negligible influence of the inflow on the detrusor's tensile stress and pressure, it is assumed that $Q_{\text{in}} = 0$ [9].

Additionally, the subsequent change occurs when the detrusor tensile stress takes into account $\sigma_{\text{lpas}D}$ and $\sigma_{\text{upas}D}$, which are the elastic and visco-elastic elements of the bladder wall.

Algorithm 4 p_D

function $p_D(V_B, f^*_{aD}, Q)$
- $r_{\text{out}D} = \left(\frac{3}{4\pi}(V_B + V_{\text{tissue}D} + V_{\text{muscle}D})\right)^{1/3}$
- $r_{\text{in}D} = \left(\frac{3}{4\pi}(V_B + V_{\text{tissue}D})\right)^{1/3}$
- $r_D = \frac{r_{\text{out}D} + r_{\text{in}D}}{2}$
- $u_D = \frac{Q}{8\pi r_{\text{opt}D}} \left(\frac{1}{r^2_{\text{out}D}} + \frac{1}{r^2_{\text{in}D}} \right)$
- $u^*_D = \frac{u_D}{u_{\text{max}D}}$
- $\sigma_{u^*_D} = \sigma_{uS}(u^*_D)$
- $l_D = \frac{l_{\text{opt}D}}{r_{\text{opt}D}} \cdot r_D$
- **if** $r_D < r_0 D$ **then**
  - $\sigma_{\text{lpas}D} = 0$
- **else**
  - $\sigma_{\text{lpas}D} = C_l \cdot \left(\frac{r_D - r_{0D}}{r_{0D}} \right)^{\alpha}$
- **end if**
- $\sigma_{\text{nom}D} = f^*_{aD} \cdot \sigma_{\text{iso}D} \cdot \sigma_{u^*_D} \cdot \sigma_{lD^*}(l_D) + \sigma_{\text{lpas}D} + \sigma_{\text{upas}D}(u^*_D)$
- $A_D = \pi(r^2_{\text{out}D} - r^2_{\text{in}D})$
- $\sigma_D = \frac{A_{\text{nom}D}}{A_D} \cdot \sigma_{\text{nom}D}$
- $p_D = \sigma_D \cdot \ln\left(\frac{r_{\text{out}D}}{r_{\text{in}D}} \right)$
- **return** p_D

end function

4.3.7 Urethral objective function, f_0

The objective function (f_0) returns the different in pressure between pressure at the entrance of the urethra and the pressure within the urethra ($p_T - p_S$). It considers various factors, including bladder volume (V_B), muscle contraction strength in the bladder wall (f^*_{aD}), sphincter muscle resistance (f^*_{aS}), and urethral radius (r_U).

The initial stage entails the computation of areas pertaining to the urethral opening, the bladder neck, and the cross-sectional area of the urethra encompassed by urine. The calculations depend on the given urethral radius (r_U) and predefined constants for the difference between radius in the urethra-bladder transition zone (δr) and bladder neck opening radius (r_{BN}).

The sphincter pressure (p_S), square rate of outflow (Q^2), and detrusor pressure (p_D) can then be obtained using the methods explained in section 4.3.4, section 4.3.5, and section 4.3.6, respectively.

Using the newly calculated data and Bernoulli's law, the pressure at the bladder neck (p_{BN}) can be computed. This involves subtracting a pressure value from the detrusor pressure. The pressure reduction is caused by an increased flow and is calculated using urine density, urine flow rate, and the areas of the relevant places in the bladder.

A similar approach is applied to acquire the pressure at the entrance of the urethra. However, there is the additional possibility of a further reduction in pressure due to tissue pressing on the bladder neck opening. The pressure loss depends on the pressure at the bladder neck opening, a constant, and the relative difference between the surface area of the bladder urine sphere and the cross-sectional area of the bladder neck opening.

Subsequently, the algorithm calculates the difference between the pressure at the entrance of the urethra and the pressure at the urethral surface. This value represents the pressure difference of interest to be used in the optimisation function.

Algorithm 5 f_0

function $f_0(V_B, f^*_{aD}, f^*_{aS}, r_U)$
$A_U \leftarrow \pi r_U^2$
$A_T \leftarrow \pi(r_U + \Delta r)^2$
$A_{BN} \leftarrow \pi r_{BN}^2$
$r_{inD} \leftarrow \left(\frac{3}{4\pi}(V_B + V_{\text{tissueD}})\right)^{1/3}$
$A_{inD} \leftarrow 4\pi r_{inD}^2$
$p_S \leftarrow p_S(A_U, f^*_{aS}, r_U)$
$Q^2 \leftarrow Q^2(A_U, A_T, p_S)$
$p_D \leftarrow p_D(V_B, f^*_{aD}, \sqrt{Q^2})$
$p_{BN} \leftarrow p_D - \frac{\rho Q^2}{2}\left(\frac{1}{A_{BN}^2} - \frac{1}{A_{inD}^2}\right)$
$r_B \leftarrow \left(\frac{3V_B}{4\pi}\right)^{1/3}$
$A_B \leftarrow 4\pi r_B^2$
if tissue pressed in bladder neck **then**
$\Delta p \leftarrow C_p p_{BN}\left(\frac{A_{BN} - A_B}{A_{BN}}\right)^2$
else
$\Delta p \leftarrow 0$
end if
$p_T \leftarrow p_D - \frac{\rho Q^2}{2A_T^2} - \Delta p$
return $p_T - p_S$
end function

4.4 Updating urine outflow

Algorithm Algorithm 6 showcases the urine outflow update function (Q), which serves as a prime example of the core design principle employed in this LUT model: modular calculation through the abstraction of complex relationships.

This algorithm leverages the modular functions which calculate sphincter pressure (p_S) and the square outflow of urine (Q^2), which are both dependent on the urethral radius (r_U) to focus on the impact of the urethral radius on the new urine flow rate. This approach offers several advantages.

By separating pressure and flow rate calculations into dedicated functions (section 4.3.4 and section 4.3.5), the model promotes modular design and code reusability. In the event of future enhancements to the model, modifications can be made to these fundamental relationships without impacting the core logic. In addition, this abstraction enables the function to show the connection between the urethral radius and the resultant flow rate, thereby enhancing the code's readability and maintainability.

The operation of the function is performed through a sequence of steps. Initially, it computes the cross-sectional area of the urethral entrance and the cross-sectional area of the urethral urine, both dependent on the radius of the urethra (r_U). Second, it leverages the pre-defined relationship between sphincter pressure, urethral area,

sphincter activation state (f^*_{aS}), and the urethral radius (section 4.3.4) to determine the sphincter pressure (p_S). Then, it utilises the pre-defined relationship between flow rate, urethral area, total outflow area, and sphincter pressure (section 4.3.5) to calculate the square flow rate (Q^2). Finally, the square root is then taken to obtain the updated urine flow rate (Q).

Algorithm 6 Q

function $Q(f^*_{aS}, r_U)$
$A_T \leftarrow \pi(r_U + \Delta r)^2$
$A_U \leftarrow \pi r_U^2$
$p_S \leftarrow p_S(A_U, f^*_{aS}, r_U)$
$Q^2 \leftarrow Q^2(A_U, A_T, p_S)$
return $\sqrt{Q^2}$
end function

4.5 Updating bladder volume

The model's final component is centred on calculating and integrating the urine's net flow into the bladder volume. The net flow is determined by Algorithm Algorithm 7 (f_1 in the model).

As stated before, the inflow rate (Q_{in}) remains constant and represents the average urine production. However, this inflow is regulated during voiding to mimic physiological patterns.

Using the function described in section 4.3.6, the algorithm calculates the detrusor pressure (p_D) by considering the bladder volume (V_B), normalized detrusor activation state (f^*_{aD}), and outflow rate (Q). This detrusor pressure represents the pressure exerted by the bladder wall to expel urine.

Then, the pressure is compared to a threshold pressure (p_θ). This threshold pressure represents the minimum pressure required to initiate voiding. If the detrusor pressure falls below the threshold ($p_D < p_\theta$), the inflow rate (Q_{in}) remains at the constant value (C_{Qin}). This represents the continuous production of urine in the bladder. Conversely, if the detrusor pressure exceeds the threshold ($p_D \geq p_\theta$), the inflow rate is set to zero ($Q_{\text{in}} = 0$). The cessation of inflow emulates the prevention of additional urine entering the bladder during voiding.

Algorithm 7 f_1

function $f_1(V_B, f^*_{aD}, Q)$
  $p_D \leftarrow p_D(V_B, f^*_{aD}, Q)$
  if $p_D < p_\theta$ **then**
    $Q_{\text{in}} \leftarrow C_{\text{Qin}}$
  else
    $Q_{\text{in}} \leftarrow 0$
  end if
return $Q_{\text{in}} - Q$
end function

The algorithm concludes by calculating the net urine flow through the subtraction of the outflow rate (Q) from the adjusted inflow rate (Q_{in}). This net flow value represents the change in bladder volume over a specific time interval.

The bladder volume (V_B) is updated based on the calculated net flow (f_1) through the use of the following equation:

$$V_B(t + \Delta t) = V_B(t) + f_1(t)\Delta t \tag{4.12}$$

Here, t represents the current time, Δt represents a small time step, and $V_B(t + \Delta t)$ represents the updated bladder volume at the next time step.

Chapter 5

Model results and development

5.1 Initial model behaviour

Figure 5.1 illustrates the resulting model, while Figure 5.2 provides a magnified view of the voiding phase. This shows that the model can successfully store and void urine. In addition, the pressure trend observed during the voiding cycle validates the implementation by matching the findings of the original paper [9]. The outflow of urine, represented by Q, demonstrates an increase in response to pressure. Conversely, the inflow of urine remains consistent and stops when voiding occurs and the pressure exceeds the threshold, in accordance with the design.

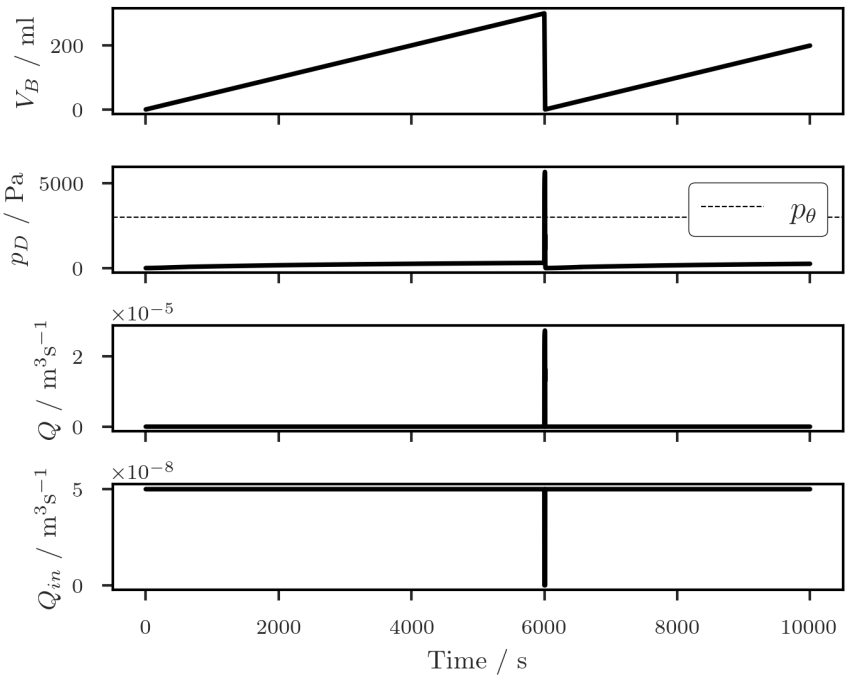

Figure 5.1: Simulation of the lower urinary tract model showing bladder volume V_B, detrusor pressure p_D, urine outflow Q, and urine inflow Q_{in} during one cycle of storage and voiding. Pressure threshold p_{θ} is denoted by a horizontal dashed line.

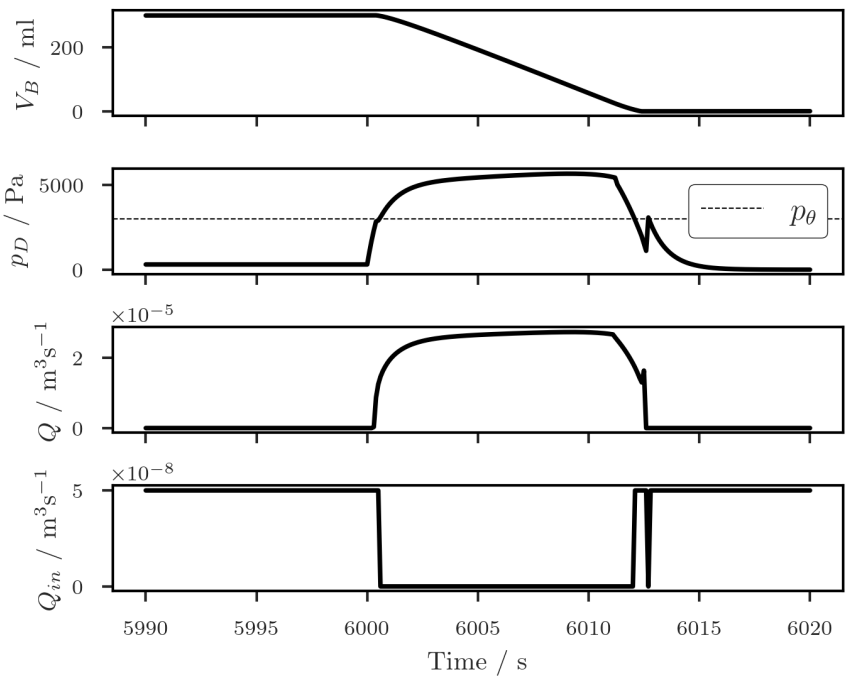

Figure 5.2: Simulation of the lower urinary tract model showing bladder volume V_B, detrusor pressure p_D, urine outflow Q, and urine inflow Q_{in} during voiding event. Pressure threshold p_{θ} is denoted by a horizontal dashed line.

5.2 Periodic bladder inflow

The current bladder inflow behaviour assumes a steady urine flow rate from the kidneys to the bladder. Modelling the state of kidney outflow for an individual is challenging because of factors such as liquid intake, food consumption, medications, other medical conditions, age, and perspiratory behaviour [33]. As a result, the current model, which assumes a constant inflow rate, is a fair assumption and can be conveniently changed for a patient if a flow test is administered. Unfortunately, this outcome creates a highly deterministic system with no variation, making it impractical for a biological system which is naturally variate.

Given the intricate nature of the factors discussed, it would not be feasible to implement or validate a kidney model relying on these factors. However, there is one factor that universally affects bladders: time. Although the production of urine in the kidneys does not change intensely throughout the day, it has been shown that numerous functions of the kidney, including urine production, vary with circadian rhythm [34, 35].

Based on this information, the inflow (Q_{in}) has been represented mathematically as a sinusoidal function, as depicted in Figure 5.3. As there is insufficient public data on per minute urine production, the function was fit to align with an average inflow that experiences fluctuations over a 24-hour cycle within ranges of typical urine production. With that in mind, the numbers provided can be adjusted and personalised, thereby enhancing the model's compatibility with users. Figure 5.3 illustrates the observed peaks in urine production during the afternoon and weaker inflow during the early

morning, aligning with what is reported in the literature [34]. Furthermore, the data indicates that the number of voiding cycles remains consistent with a healthy number of cycles per day [36].

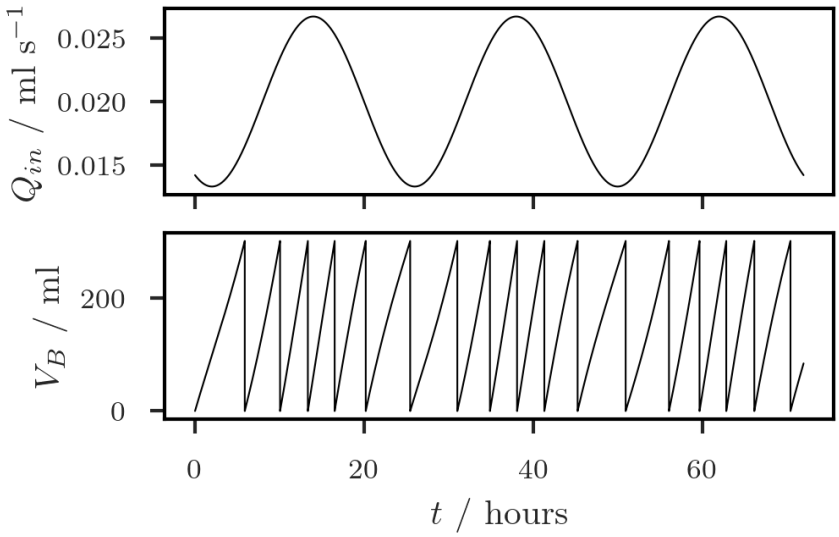

Figure 5.3: Sinusoidal filling rate of bladder

Despite its increased complexity, this model of urine production can still be adjusted with just a few parameters if there were a significant difference between a patient's flow rates and the current model.

5.3 Stochastic bladder inflow

The previous section introduced the idea of circadian rhythm in urine production, which is represented in the model as a sinusoidal function. Although this approach demonstrates the cyclical nature of bladder filling, it fails to incorporate the inherent variability present in biological systems. In order to make the model more realistic, a stochastic component is introduced through the injection of noise.

It is uncommon for biological processes to display complete periodicity. Inherent noise in physiological systems arises from factors including individual variations, hormonal fluctuations, and dietary intake [35].

Moreover, introducing a stochastic component could offer an advantage for future research. This is because a non-deterministic wave might challenge the learning capacity of connected neural circuits when fitting more complex data compared to the previous model.

In order to overcome this constraint, random noise is introduced into the incoming flow. After each minute (or chosen time step), a random scalar uniformly distributed between -1 and 1 is multiplied by the volume obtained from the sine function. The bounds were manually adjusted and serve as an estimation of noise, however, a more

data-driven analysis based on a larger dataset could fine-tune these parameters. This method preserves the overall circadian pattern while introducing controlled variability.

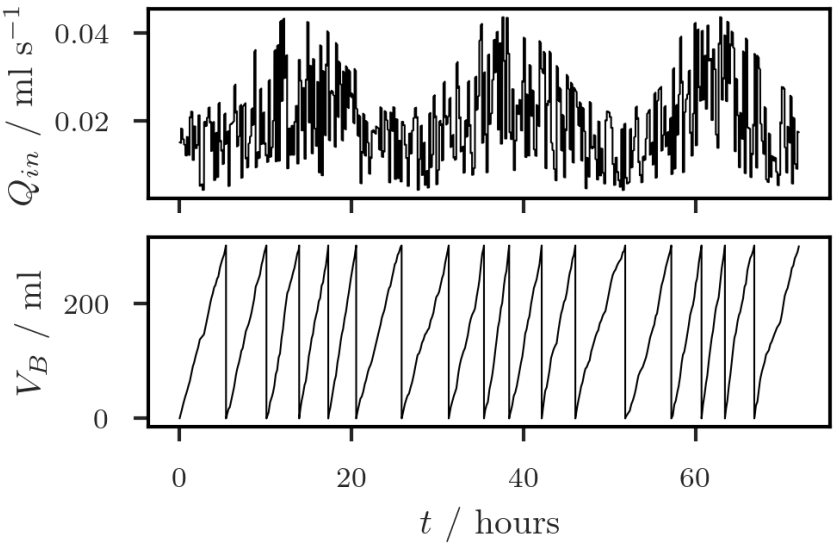

Figure 5.4: Stochastic sinusoidal filling rate of bladder

The absence of an exact period is evident in Figure 5.4, signifying that each set of data for a given time can be deemed unique within the context of this model. Nevertheless, the filling model continues to demonstrate the general circadian trend as a result of the underlying sinusoidal function.

Chapter 6

Discussion

6.1 Key findings and model performance

Chapter 4 details the successful replication and enhancement of a lower urinary tract model. The inclusion of sinusoidal kidney function altered the filling rate to be non-constant and varied the intervoid interval to better reflect human biology. Furthermore, by introducing noise, a stochastic filling rate was achieved that preserves the underlying patterns while creating a non-constant time period and random intervoid interval, mirroring the unpredictable nature of biological systems.

Validating a biophysical model of the lower urinary tract (LUT) is a challenging task. In an ideal scenario, the validation process of the model would consist of a direct comparison between its outputs and data obtained from human clinical studies. However, the acquisition of high-quality data pertaining to bladder pressure, volume, and voiding dynamics frequently involves invasive measures. Moreover, ethical considerations constrain the scope of experiments that can be undertaken on individuals who are in a state of good health. Even with access to patient data, the variations in anatomy, physiology, and medical conditions among individuals can pose challenges in attaining an exact correspondence between model predictions and actual observations. Even in cases where human data exists, researchers do not share it publicly because of privacy laws and ethics, hindering the reproducibility of validation results.

Consequently, researchers often validate specific components of a model by comparing them to data obtained from animal studies or in vitro experiments. This entails employing a variety of methods, such as comparing against established physiological ranges, reproducing published model outputs, and examining model behavior during well-understood physiological perturbations.

6.1.1 Pressure-Volume relationship

While the implementation aligns with the original paper [9] in terms of pressure, volume, and neural fire frequencies, there are discrepancies between certain aspects of the model and the published literature. For instance, when evaluating the pressure of the detrusor

muscle while the bladder is being filled (Figure 6.1), the present contraction rate is too high, causing an abrupt rise in pressure that exceeds normal thresholds.

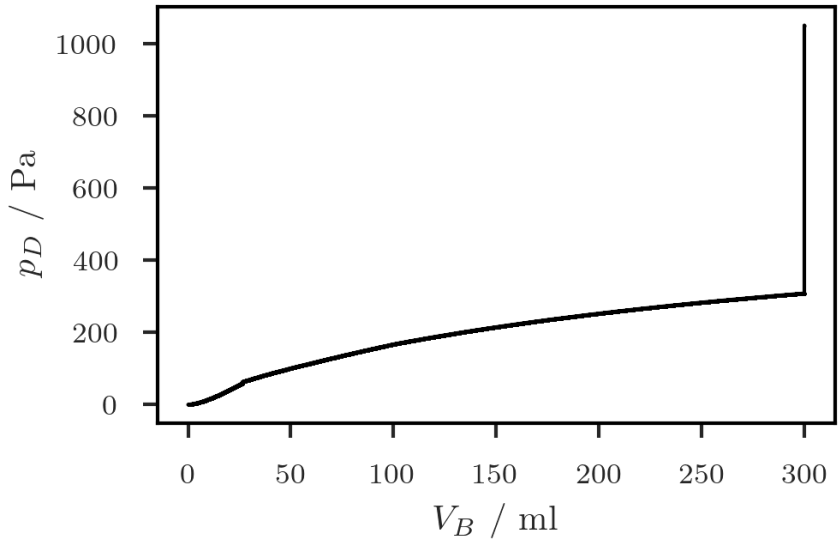

Figure 6.1: Pressure-volume relationship during filling.

The initial assumption was that the problem does not lie with the model itself, but rather with the simplified neural control model. To assess this, modifications were applied to the neural circuit. This included the utilisation of Gaussian functions to model the spike in neural activity, resulting in a smoother increase in pressure during the filling phase.

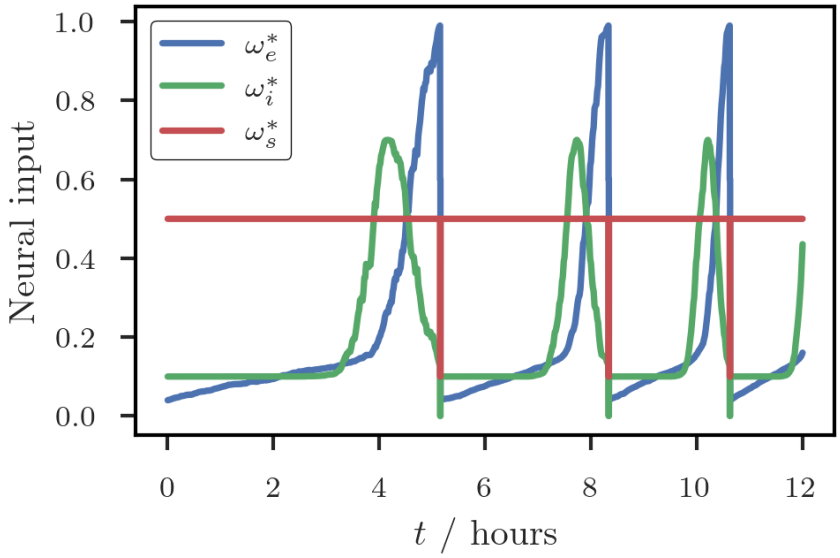

Figure 6.2: Updated neural inputs using Gaussian model

Figure 6.2 displays the updated neural weights. The modification in the neural weights' interaction with the model leads to a gradual rise in pressure, as depicted in Figure 6.3.

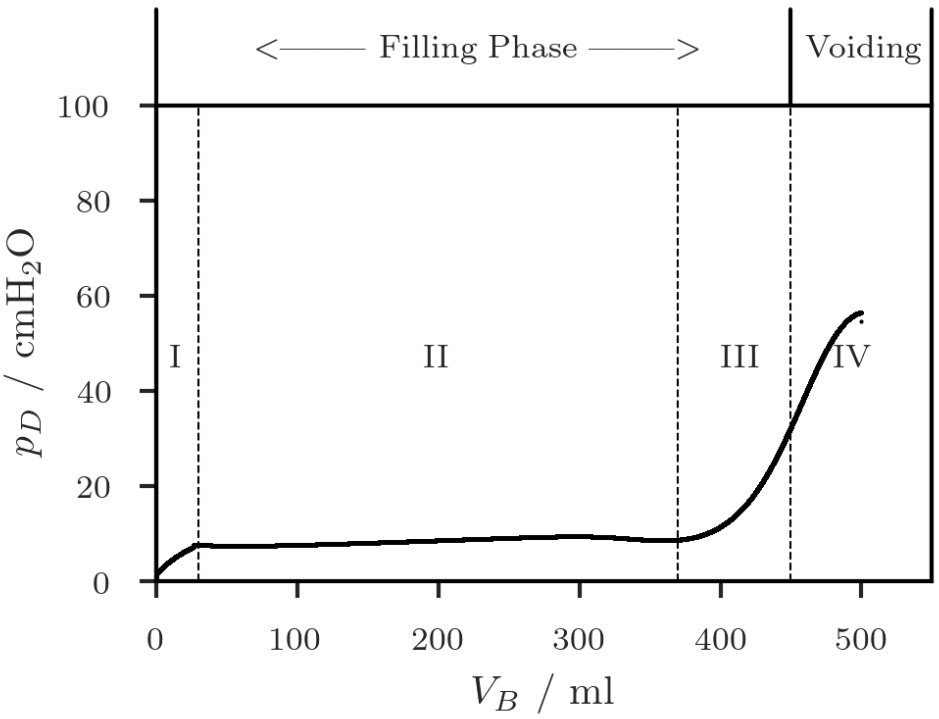

Figure 6.3: Updated pressure-volume relationship using Gaussian neural firing model

Consequently, the relationship between pressure and volume shows a less pronounced slope. To facilitate comparison with literature, the detrusor pressure in this figure has been converted to units of cmH_2O. The pressure-volume plot exhibits a close resemblance to an ideal cystometrogram of a typical adult human female [37], characterised by an initial rise in pressure during phase I, subsequent bladder compliance in phase II, and concluding with a gradual pressure increase and voiding during phases III-IV.

6.1.2 Bladder compliance

During phase II of Figure 6.3, the bladder exhibits compliance as it stretches with minimal increase in detrusor pressure. For a bladder to be considered normal, its compliance should be over $40\,mL/cmH_2O$ [38]. Since each voiding cycle is no longer deterministic, a simulation was conducted to determine compliance in each filling cycle. Figure 6.4 displays the results, indicating that compliance exceeds $40\,mL/cmH_2O$ in all cycles, demonstrating a healthy bladder.

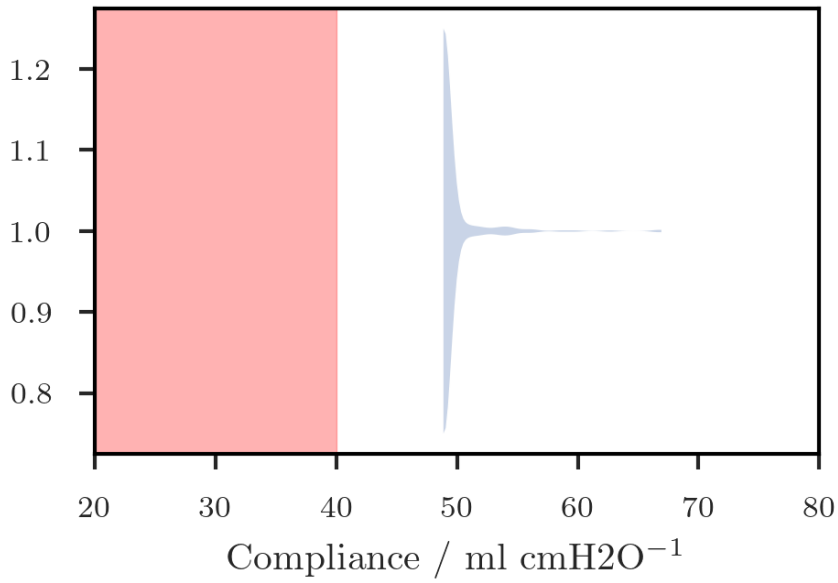

Figure 6.4: Violin plot showing distribution of compliance values during each filling cycle.

6.1.3 Intervoid interval

The initial model maintained a constant intervoid interval within the healthy range. The changes to the model now lead to a variable interval, requiring the model to run over 50 days to extract the interval from each void cycle. For the purposes of grouping the intervals, it was assumed that night falls between 10pm and 6am, however this will vary depending on the sleep cycle of the individual.

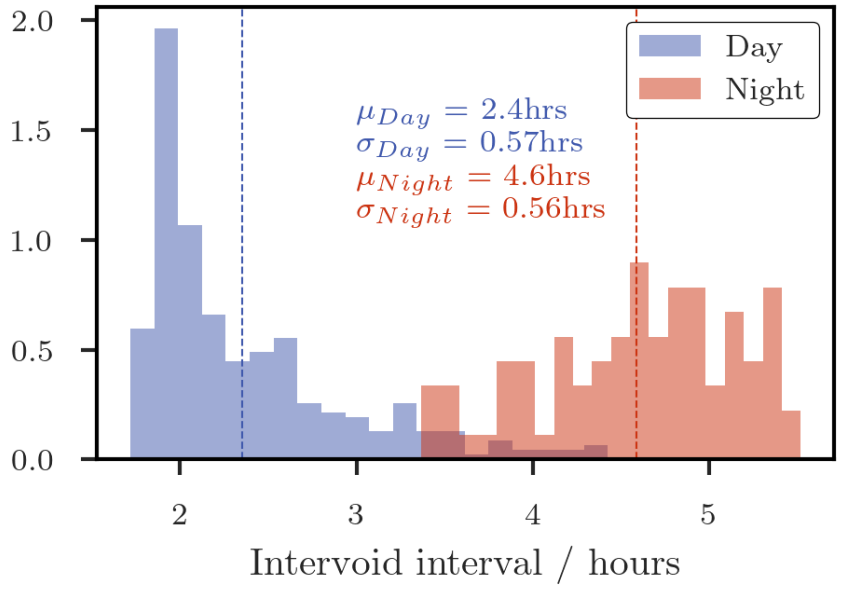

Figure 6.5: Histogram showing distribution of intervoid intervals.

Figure 6.5 displays the distribution of time intervals between voiding events. Majority of the cycles during the day align with the 3-4 hour time period as mentioned in the literature [39, 36]. On the other hand, the night voids seem to be shorter than expected, with the model consistently experiencing at least one void at night. Although this is not uncommon, it could indicate that the filling model needs to be revised beyond a singular sine curve.

6.1.4 Voiding duration

Alongside the assessment of the intervoid interval, the investigation also explored the distribution of voiding durations over the course of the 50-day simulation. As illustrated in Figure 6.6, each voiding event exhibited a duration of approximately 27 seconds, independent of the preceding bladder filling time. Previous research suggests an average voiding duration of 21 ± 13 seconds [40]. While the value in this simulation exceeded the expected duration slightly, it remained within the range established by the literature. The previous neural firing model used in the framework showed a similar distribution, but with a shorter voiding duration centred around 16 seconds. The observed difference suggests that modifications to the neural control model may be required for improved synchronisation with the voiding dynamics depicted in the current model. The LUT model itself, however, appears to be functioning within a physiologically relevant range.

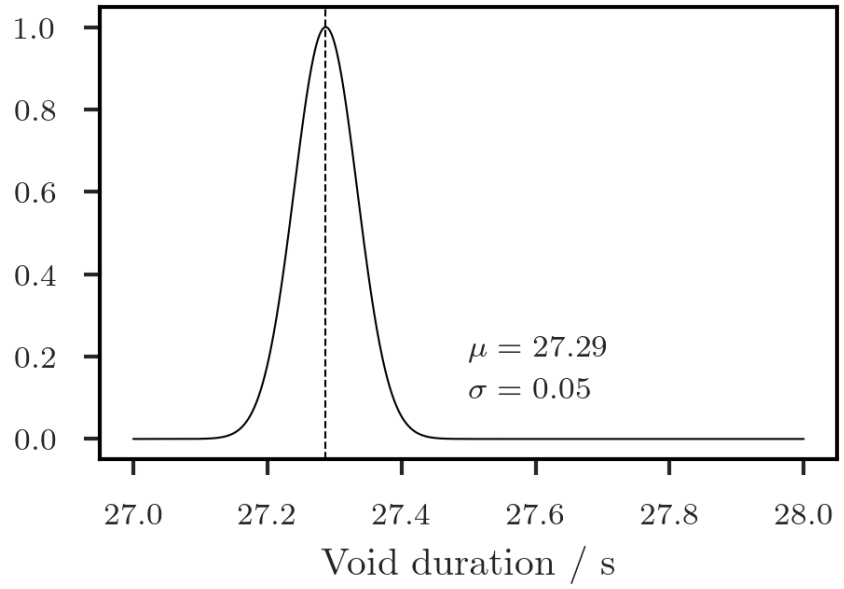

Figure 6.6: Distribution of voiding duration.

6.1.5 Rat data comparison

Utilising data obtained from rat experiments [18], a two-step validation was employed to assess the lower urinary tract model's ability to represent real-world physiology. First, min-max scaling was applied to the rat data to bring it into a range comparable with the predictions of the human model. This allowed for a visual overlay of the scaled rat data

onto the model's outputs. This qualitative comparison provided valuable insights into the similarity between the model's behaviour and the actual observations from the rat experiments.

Secondly, a quantitative analysis using Pearson correlation was conducted. In this case, the non-scaled rat data was compared with the corresponding outputs from the human model. The relationship of P/V was used as a metric to compare.

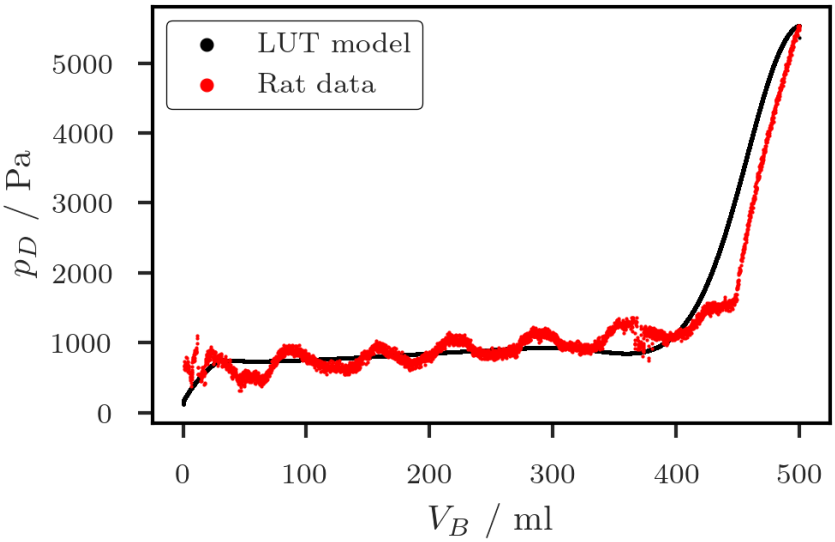

Figure 6.7: Pressure-volume relationship for scaled rat data and LUT model.

The scaled rat data in Figure 6.7 exhibited high similarity when overlaid on the human model outputs. This suggests the model effectively captures the general trends observed in the rat experiments. Further strengthening this validation, the Pearson correlation coefficient between the non-scaled rat data and the model outputs yielded a statistically significant value of 0.93 ($p < 0.001$). This high correlation value highlights a strong positive relationship between the model's predictions and the in-vivo data, providing further confidence in the model's accuracy.

However, the rat data does demonstrate fluctuations during the compliance phase of storage. This could be due to muscle spasms or noise produced in the recording of the small pressure values.

6.2 Limitations

The current LUT model relies on several assumptions inherited from gaps in the original reference paper. These assumptions, such as the tensile stress-length relationship, may not precisely reflect the complexities of real-world physiology. Additionally, the neural and kidney models within the LUT system utilise approximated parameters, which could benefit from further refinement.

The rat data used for validation, while valuable, revealed fluctuations during compliance measurements. It's important to note that these fluctuations might not be a limitation of the LUT model itself. The limitations could lie with the recording instruments used in the rat experiments or even the process of filling the rat bladder. Moreover, these fluctuations might not be representative of what happens in a human bladder due to the capacity difference.

Exploring these limitations provides promising opportunities for future research.

6.3 Future work

There are multiple options available for advancing and improving the current LUT model. By incorporating these advancements, the model's capabilities can be enhanced and its applications can be broadened.

6.3.1 Refining model parameters

The analysis of voiding duration reveals that modifications to the neural control model may be required. Additionally, other model parameters, such as the weight of the noise during bladder filling, should be tuned to ensure the model is as accurate as possible. The goal of these adjustments is to achieve a more effective synchronisation with the voiding dynamics captured by the current LUT model. Future studies could focus on particular areas for improvement, including the incorporation of additional neural feedback mechanisms or the optimisation of parameters governing neural firing patterns.

Depending on the particular research emphasis, the model may be extended to incorporate further physiological details. This could involve the integration of urethral resistance dynamics, a more detailed modelling of the micturition reflex, or including age-related physiological changes.

6.3.2 Model validation

The acquisition of human data is important for achieving conclusive validation. Future research should prioritise the acquisition of such data while ensuring adherence to ethical and privacy considerations. The facilitation of this process could be achieved through collaboration with clinical researchers and healthcare professionals.

Apart from relying on in vivo data, other validation techniques can be investigated. Possible options could involve conducting in vitro experiments on isolated tissue samples of the LUT or comparing simulation results with established models to cross-validate. Although it would be a time-consuming task, this could be a feasible choice if there were a lack of available supplementary data.

6.3.3 Applications of the model

The model's capability to simulate OAB presents avenues for exploring its mechanisms and potential treatments. Future work could identify primary parameters that exhibit

high correlation with OAB and establishing their ranges through literature or physiological principles. These parameters should then be systematically adjusted to simulate various degrees of OAB severity. The analysis of the resulting voiding patterns would explain how the model captures variations in OAB.

In order to utilise the model effectively, further research will focus on integrating it into the neural firing circuit developed by another member of the lab (as previously described in section 2.2). By combining the biophysical model and a neural firing network, this integration offers a chance to create a more comprehensive LUT function model which can generate new results indefinitely. This combined model would be an improvement over the current circuit which depends on finite pre-recorded data. However, the key to successful integration lies in addressing the compatibility between the two models. More precisely, the firing rates of the afferent and efferent pathways in the neural circuit will need to be transformed in order to meet the input and output criteria of the current LUT model. This conversion process might involve scaling or transforming the firing rates to neural inputs used within the LUT model, which can be calibrated using rodent pressure and volume data.

Chapter 7

Conclusion

This project was able to successfully implement and develop a model of the lower urinary tract. By incorporating sinusoidal kidney function and noise injection, a more realistic model was achieved that accurately represents the dynamic filling rate and unpredictable behaviour of the biological system. Validation of the model was performed, confirming its results by comparing to established physiological ranges and published literature on bladder compliance and voiding intervals.

Based on the performance across multiple metrics, it can be concluded that the model's functionality is consistent with established physiological principles. However, some variations observed in results highlight the potential for further refinement. The successful development of a biophysical LUT model lays the groundwork for further integration with the existing neural firing circuit. This combined model has the potential to create a comprehensive representation of LUT function, paving the way for a deeper understanding of neural and biomechanical interactions within the lower urinary tract.

Bibliography

[1] D. E. Irwin, I. Milsom, S. Hunskaar, K. Reilly, Z. Kopp, S. Herschorn, K. Coyne, C. Kelleher, C. Hampel, W. Artibani, and et al., "Population-based survey of urinary incontinence, overactive bladder, and other lower urinary tract symptoms in five countries: Results of the epic study," *European Urology*, vol. 50, no. 6, p. 1306–1315, Dec 2006.

[2] M. K. Kim, Y. S. Shin, J. H. Lee, W. J. Cho, and D. K. Kim, "The prevalence of lower urinary tract symptoms and overactive bladder in south korea: A cross-sectional, population-based study," *International Neurourology Journal*, vol. 26, no. 1, p. 31–36, Mar 2022.

[3] Royal United Hospitals Bath NHS Foundation Trust, "Overactive Bladder Syndrome (OAB)," October 2023, Accessed: Oct. 18, 2023. [Online]. Available: https://www.ruh.nhs.uk/patients/Urology/documents/patient_leaflets/UR0043_Overactive_Bladder_Syndrome.pdf

[4] D. E. Irwin, Z. S. Kopp, B. Agatep, I. Milsom, and P. Abrams, "Worldwide prevalence estimates of lower urinary tract symptoms, overactive bladder, urinary incontinence and bladder outlet obstruction," *BJU International*, vol. 108, no. 7, pp. 1132–1138, 2011. [Online]. Available: https://onlinelibrary.wiley.com/doi/abs/10.1111/j.1464-410X.2010.09993.x

[5] P. Nicolson, Z. Kopp, C. R. Chapple, and C. Kelleher, "It's just the worry about not being able to control it! a qualitative study of living with overactive bladder," *British Journal of Health Psychology*, vol. 13, no. 2, p. 343–359, May 2008.

[6] Wrightington, Wigan and Leigh Teaching Hospitals NHS Foundation Trust, "Treatments for Overactive Bladder," January 2023, Accessed 25 March 2024. [Online]. Available: https://www.wwl.nhs.uk/media/.leaflets/63ce4cd4cb9019.65411105.pdf

[7] UK Parliament, "Overactive bladder syndrome," Jan 2022, https://edm.parliament.uk/early-day-motion/59326/overactive-bladder-syndrome. [Online]. Available: https://edm.parliament.uk/early-day-motion/59326/overactive-bladder-syndrome

[8] A. Astasio-Picado and M. García-Cano, "Neuromodulation of the posterior tibial nerve for the control of urinary incontinence," *Medicina*, vol. 58, no. 3, p. 442, Mar 2022.

[9] E. H. Bastiaanssen, J. L. van Leeuwen, J. Vanderschoot, and P. A. Redert, "A myocybernetic model of the lower urinary tract," *Journal of Theoretical Biology*, vol. 178, no. 2, pp. 113–133, Jan. 1996.

[10] D. Jaskowak, R. Nunez, R. Ramachandran, E. Alhajjar, J. Yin, G. Guidoboni, and Z. C. Danziger, "Mathematical modeling of the lower urinary tract: A review," *Neurourology and Urodynamics*, vol. 41, no. 6, p. 1305–1315, 2022.

[11] B. Abelson, D. Sun, L. Que, R. A. Nebel, D. Baker, P. Popiel, C. L. Amundsen, T. Chai, C. Close, M. DiSanto, M. O. Fraser, S. J. Kielb, G. Kuchel, E. R. Mueller, M. H. Palmer, C. Parker-Autry, A. J. Wolfe, and M. S. Damaser, "Sex differences in lower urinary tract biology and physiology," *Biology of Sex Differences*, vol. 9, no. 1, p. 45, Oct. 2018. [Online]. Available: https://doi.org/10.1186/s13293-018-0204-8

[12] W. C. de Groat, D. Griffiths, and N. Yoshimura, "Neural Control of the Lower Urinary Tract," in *Comprehensive Physiology*. John Wiley & Sons, Ltd, 2014, pp. 327–396. [Online]. Available: https://onlinelibrary.wiley.com/doi/abs/10.1002/cphy.c130056

[13] A. K. Patel and C. R. Chapple, "Anatomy of the lower urinary tract," *Surgery (Oxford)*, vol. 26, no. 4, pp. 127–132, Apr. 2008. [Online]. Available: https://www.sciencedirect.com/science/article/pii/S0263931908000471

[14] P. Sam, A. Nassereddin, and C. A. LaGrange, "Anatomy, Abdomen and Pelvis: Bladder Detrusor Muscle," in *StatPearls*. Treasure Island (FL): StatPearls Publishing, 2024. [Online]. Available: http://www.ncbi.nlm.nih.gov/books/NBK482181/

[15] J. Jung, H. K. Ahn, and Y. Huh, "Clinical and Functional Anatomy of the Urethral Sphincter," *International Neurourology Journal*, vol. 16, no. 3, pp. 102–106, Sep. 2012. [Online]. Available: https://www.ncbi.nlm.nih.gov/pmc/articles/PMC3469827/

[16] BioRender, "Scientific image and illustration software." [Online]. Available: https://www.biorender.com/

[17] W. C. de Groat and C. Wickens, "Organization of the neural switching circuitry underlying reflex micturition," *Acta Physiologica (Oxford, England)*, vol. 207, no. 1, pp. 66–84, Jan. 2013.

[18] M. Jabbari and A. Erfanian, "Estimation of bladder pressure and volume from the neural activity of lumbosacral dorsal horn using a long-short-term-memory-based deep neural network," *Scientific Reports*, vol. 9, no. 1, Dec 2019.

[19] E. Bastiaanssen, J. Van Leeuwen, J. Vanderschoot, and P. Redert, "A myocybernetic model of the lower urinary tract," *Journal of theoretical biology*, vol. 178, no. 2, pp. 113–133, 1996.

[20] F. A. Valentini, G. R. Besson, P. P. Nelson, and P. E. Zimmern, "A mathematical micturition model to restore simple flow recordings in healthy and symptomatic individuals and enhance uroflow interpretation," *Neurourology and Urodynamics:*

Official Journal of the International Continence Society, vol. 19, no. 2, pp. 153–176, 2000.

[21] R. A. Hosein and D. J. Griffiths, "Computer simulation of the neural control of bladder and urethra," *Neurourology and Urodynamics*, vol. 9, no. 6, pp. 601–618, 1990.

[22] F. Van Duin, P. Rosier, N. Rijkhoff, P. Van Kerrebroeck, F. Debruyne, and H. Wijkstra, "A computer model of the neural control of the lower urinary tract," *Neurourology and Urodynamics: Official Journal of the International Continence Society*, vol. 17, no. 3, pp. 175–196, 1998.

[23] W. Fletcher, F. Smith, and C. Fry, "A computer simulation of micturition," 2005. [Online]. Available: http://abacus.gene.ucl.ac.uk/will/files/micturition.pdf

[24] U. Hübener and R. van Mastrigt, "Computer simulation of micturition," *Urodinamica*, vol. 4, pp. 81–90, 1994.

[25] A. S. Paya, D. R. Fernandez, D. Gil, J. M. Garcia Chamizo, and F. M. Perez, "Mathematical modelling of the lower urinary tract," *Computer Methods and Programs in Biomedicine*, vol. 109, no. 3, p. 323–338, Mar 2013.

[26] E. Bastiaanssen and J. Van Leeuwen, "Neural control model for the lower urinary tract," in *Proceedings of the Artificial Neural Networks in Engineering Conference (ANNIE'94)*, Dec. 1994, pp. 579–584, Conference date: 13-11-1994 Through 16-11-1994.

[27] SciPy, "scipy.optimize.bisect — SciPy v1.12.0 Manual," https://docs.scipy.org/doc/scipy/reference/generated/scipy.optimize.bisect.html. [Online]. Available: https://docs.scipy.org/doc/scipy/reference/generated/scipy.optimize.bisect.html

[28] J. L. Krans, "Sliding Filament Theory," https://www.nature.com/scitable/topicpage/the-sliding-filament-theory-of-muscle-contraction-14567666/. [Online]. Available: https://www.nature.com/scitable/topicpage/the-sliding-filament-theory-of-muscle-contraction-14567666/

[29] J. L. van Leeuwen, "Optimum power output and structural design of sarcomeres," *Journal of Theoretical Biology*, vol. 149, no. 2, pp. 229–256, Mar. 1991. [Online]. Available: https://www.sciencedirect.com/science/article/pii/S0022519305802796

[30] A. V. Hill, "The heat of shortening and the dynamic constants of muscle," *Proceedings of the Royal Society of London. Series B - Biological Sciences*, vol. 126, no. 843, pp. 136–195, Jan. 1997, publisher: Royal Society. [Online]. Available: https://royalsocietypublishing.org/doi/10.1098/rspb.1938.0050

[31] X. Aubert, *Le Couplage énergétique de la contraction musculaire*. Éditions Arscia, 1956. [Online]. Available: https://books.google.co.uk/books?id=A5XHXwAACAAJ

[32] B. Kumari and N. Kumar, "Principle of bernoulli's equation and its applications," *NeuroQuantology*, vol. 20, no. 10, p. 5078–5084, 2022.

[33] National Institute of Diabetes and Digestive and Kidney Diseases, "The Urinary Tract & How It Works - NIDDK," Jun. 2020, https://www.niddk.nih.gov/health-information/urologic-diseases/urinary-tract-how-it-works. [Online]. Available: https://www.niddk.nih.gov/health-information/urologic-diseases/urinary-tract-how-it-works

[34] I. Nakamoto, S. Uiji, R. Okata, H. Endo, S. Tohyama, R. Nitta, S. Hashimoto, Y. Matsushima, J. Wakimoto, S. Hashimoto, Y. Nishiyama, D. Kanikowska, H. Negoro, and T. Wakamura, "Diurnal rhythms of urine volume and electrolyte excretion in healthy young men under differing intensities of daytime light exposure," *Scientific Reports*, vol. 11, no. 1, p. 13097, Jun. 2021, publisher: Nature Publishing Group. [Online]. Available: https://www.nature.com/articles/s41598-021-92595-0

[35] D. Firsov and O. Bonny, "Circadian rhythms and the kidney," *Nature Reviews Nephrology*, vol. 14, no. 10, pp. 626–635, Oct. 2018, publisher: Nature Publishing Group. [Online]. Available: https://www.nature.com/articles/s41581-018-0048-9

[36] Bladder & Bowel Community, "Urinary frequency," Aug 2021. [Online]. Available: https://www.bladderandbowel.org/bladder/bladder-conditions-and-symptoms/frequency/

[37] Women's Health and Education Center (WHEC), "Uro/Gynecology - Urodynamic Assessment: Techniques," Feb. 2009, http://www.womenshealthsection.com/content/urog/urog003.php3. [Online]. Available: http://www.womenshealthsection.com/content/urog/urog003.php3

[38] X. Zhang, D. A. Husmann, L. A. Mynderse, A. Alizad, and M. Fatemi, "Non-invasive assessment of urinary bladder compliance using ultrasound: first validation study based on clinical urodynamic study," *Annals of Translational Medicine*, vol. 9, no. 7, p. 547, Apr. 2021. [Online]. Available: https://www.ncbi.nlm.nih.gov/pmc/articles/PMC8105840/

[39] Eating Well, "How Often Should You Pee & When Is It Too Much?" Aug. 2023, https://www.eatingwell.com/article/8062577/how-often-should-you-pee/. [Online]. Available: https://www.eatingwell.com/article/8062577/how-often-should-you-pee/

[40] P. J. Yang, J. Pham, J. Choo, and D. L. Hu, "Duration of urination does not change with body size," *Proceedings of the National Academy of Sciences*, vol. 111, no. 33, pp. 11 932–11 937, Aug. 2014, publisher: Proceedings of the National Academy of Sciences. [Online]. Available: https://www.pnas.org/doi/full/10.1073/pnas.1402289111